

# MULTIBAND STUDIES OF THE OPTICAL PERIODIC MODULATION IN THE X-RAY BINARY SAX J1808.4–3658 DURING ITS QUIESCENCE AND 2008 OUTBURST

ZHONGXIANG WANG<sup>1</sup>, RENE P. BRETON<sup>2,3</sup>, CRAIG O. HEINKE<sup>4</sup>, CHRISTOPHER J. DELOYE<sup>4</sup>, AND JING ZHONG<sup>1,5</sup>

*Draft version January 22, 2022*

## ABSTRACT

We report on time-resolved optical imaging of the X-ray binary SAX J1808.4–3658 during its quiescent state and 2008 outburst. The binary, containing an accretion-powered millisecond pulsar, has a large sinusoidal-like modulation in its quiescent optical emission. We employ a Markov chain Monte Carlo technique to fit our multi-band light curve data in quiescence with an irradiated star model, and derive a tight constraint of  $50^{+6}_{-5}$  deg on the inclination angle  $i$  of the binary system. The pulsar and its companion are constrained to have masses of  $0.97^{+0.31}_{-0.22} M_{\odot}$  and  $0.04^{+0.02}_{-0.01} M_{\odot}$  (both  $1\sigma$  ranges), respectively. The dependence of these results on the measurements of the companion's projected radial velocity is discussed. We also find that the accretion disk had nearly constant optical fluxes over a  $\sim 500$  day period in the quiescent state our data covered, but started brightening 1.5 months before the 2008 outburst. Variations in modulation during the outburst were detected in our four observations made 7–12 days after the start of the outburst, and a sinusoidal-like modulation with 0.2 mag amplitude changed to have a smaller amplitude of 0.1 mag. The modulation variations are discussed. We estimate the albedo of the companion during its quiescence and the outburst, which was approximately 0 and 0.8 (for isotropic emission), respectively. This large difference probably provides additional evidence that the neutron star in the binary turns on as a radio pulsar in quiescence.

*Subject headings:* binaries: close — stars: individual (SAX J1808.4–3658) — X-rays: binary — stars: low-mass — stars: neutron

## 1. INTRODUCTION

Among  $\sim 200$  known low-mass X-ray binaries (LMXBs), SAX J1808.4–3658 (hereafter J1808.4) stands out because not only was it the first discovered accretion-powered millisecond pulsar (APMP) system (Wijnands & van der Klis 1998), but also this transient system is relatively bright during quiescence and has relatively frequent outbursts, allowing detailed studies of its various properties (see Hartman et al. 2008 and references therein). One intriguing property of the system is the fact that the millisecond pulsar possibly switches its energy source from accretion during outbursts to rotation during quiescence. This possible property is indicated by bright, large-amplitude optical modulation (Homer et al. 2001; Campana et al. 2004; Deloye et al. 2008; Wang et al. 2009) seen in the binary during quiescence, which can not be caused by X-ray heating of the inner face of the companion star. The quiescent X-ray luminosity  $L_X$  ( $\simeq 5 \times 10^{31}$  erg s<sup>−1</sup>; Campana et al. 2002; Heinke et al. 2007) is two orders of magnitude lower than that required (Burderi et al. 2003). Instead, if one considers that the neutron star in the binary turns on as a radio pulsar in quiescence, its rotational energy output (so-called spin-down lumi-

nosity)  $L_{sd}$  is  $\simeq 9 \times 10^{33}$  erg s<sup>−1</sup> (Hartman et al. 2008). This energy output would presumably be in the form of a pulsar wind and sufficient to illuminate the inner face of the companion star. Among over a dozen known APMP binaries (Patruno 2010), two other systems, IGR J00291+5934 and XTE J1814–338, were also found to have similar optical modulations that cannot be explained by X-ray heating (D’Avanzo et al. 2007, 2009; however for the first source, see also Jonker et al. 2008), suggesting that APMPs in these systems might commonly switch to be radio pulsars during quiescence.

To fully examine the possibility in J1808.4, Deloye et al. (2008; see also Heinke et al. 2009) have observed J1808.4 simultaneously at X-ray and optical energies, and from the observations they have confirmed the inconsistency between the large-amplitude optical modulation and low X-ray luminosity. Applying a phase-coherent timing technique, Wang et al. (2009) have accurately determined the period and phase of the optical modulation and concluded that the optical periodicity is highly consistent with the X-ray orbital ephemeris (derived from pulsar timing; Hartman et al. 2008). Their results have excluded other possible origins (such as the accretion disk) and established that the modulation does arise from the companion star.

Following these studies, it should be interesting to compare the modulations between outburst and quiescence since presumably the former is caused by X-ray heating, and the latter by pulsar wind heating. When J1808.4 was reported to have its expected outburst (Galloway 2008) at the end of 2008 September (Markwardt & Swank 2008), we organized optical observations of the source and obtained its light curves during the outburst. In this paper, we report on the results from the observations.

<sup>1</sup> Shanghai Astronomical Observatory, Chinese Academy of Sciences, 80 Nandan Road, Shanghai 200030, China

<sup>2</sup> School of Physics and Astronomy, University of Southampton, Highfield, Southampton SO17 1BJ, U.K.

<sup>3</sup> Department of Astronomy and Astrophysics, University of Toronto, 50 St. George Street, Toronto, ON M5S 3H4, Canada

<sup>4</sup> Department of Physics, University of Alberta, Room 238 CEB, Edmonton, AB T6G 2G7, Canada

<sup>5</sup> Graduate School of Chinese Academy of Sciences, No. 19A, Yuquan Road, Beijing 100049, China

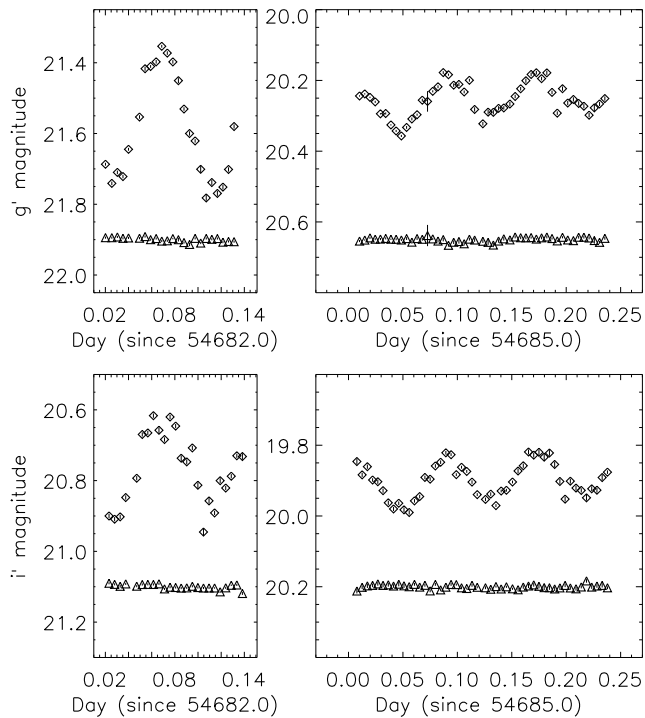


FIG. 1.— Gemini South  $g'$  (upper panels) and  $i'$  (bottom panels) light curves of J1808.4 obtained in 2008 August. Light curves of a comparison star (triangles) are also plotted.

In addition, Deloye et al. (2008) have shown that by fitting the quiescent optical modulation in J1808.4 with an advanced binary light curve model, in which lights from an accretion disk and an irradiated donor are considered, important constraints on the binary system (such as the inclination and neutron star’s mass) can be derived. Their work also concluded that in order to obtain better parameter constraints for this system, simultaneous multi-band light curves would be needed. Using data newly obtained as well as those reported in Deloye et al. (2008) and Wang et al. (2009), we have conducted fitting to the modulation. We used the binary light curve code *Icarus* (Breton et al. 2012), that is similar to the ELC program (Orosz & Hauschildt 2000) used by Deloye et al. (2008). We also employed a Markov chain Monte Carlo (MCMC) technique that allows for simultaneously fitting the multi-dimensional light curve model to the data and identifies the best-fit parameters as well as their confidence intervals.

We describe the previous light curve data, our time-resolved photometry of J1808.4 in 2008, and related data reduction in § 2. We provide details of our binary light curve model and MCMC fitting of the obtained light curves, and fitting results in § 3. Timing analysis of all the quiescent light curves and analysis of broad-band disk spectra obtained from our fitting are given in § 4. We discuss interesting results from our observations in § 5, and a summary is provided in § 6.

## 2. OBSERVATIONS AND DATA REDUCTION

### 2.1. Previous Gemini Data Obtained in Quiescence

Two sets of light curve data obtained from previous Gemini imaging observations were included in this work. The observations for the first and second set were carried

out in 2007 March and 2008 May, and were reported in Deloye et al. (2008) and Wang et al. (2009), respectively. The first set mainly contains two  $g'$  light curves, one 2.5 hour long and the other 2.8 hour long, while two additional  $i'$  brightness data points were obtained at the end of each  $g'$  light curve. The second set contains three 3 hour  $r'$  light curves obtained over 5 days. Detailed descriptions of the datasets can be found in Deloye et al. (2008) and Wang et al. (2009).

### 2.2. Gemini Imaging in 2008 August in Quiescence

Time-resolved imaging of J1808.4 was carried out with Gemini South Telescope on 2008 August 4 and 7. To obtain nearly simultaneous multi-band light curves, Sloan  $g'$  and  $i'$  filters were alternately used for imaging in each night. The detector was the Gemini Multi-Object Spectrograph (GMOS; Hook et al. 2004), which consists of three  $2048 \times 4608$  EEV CCDs. In our observations, only a section of  $300 \times 300$  pixel<sup>2</sup> in the middle CCD (CCD 02) was used. The pixel scale is  $0.073''/\text{pixel}$ .

The total observation time in the first night was 3 hours, with 23 and 24 useful  $g'$  and  $i'$  images respectively made. The exposure times were 200.5 s in  $g'$  and 150.5 s in  $i'$ . The observing conditions were variable, with the seeing [full-width half-maximum (FWHM) of the point spread function (PSF) of the images] increasing from  $0.6''$  to  $0.9''$  over the course of the observation. On August 7, the total observation time was 5.5 hours, during which 47 and 48 useful  $g'$  and  $i'$  images, respectively, were made. The exposure time at each band was the same as that in the first night. The observing conditions were relatively stable, with the average seeing being  $\simeq 0.7''$ .

### 2.3. Canada France Hawaii Telescope (CFHT) Imaging in the 2008 Outburst

The starting of the 2008 outburst of J1808.4 was reported by Markwardt & Swank (2008) on 2008 September 22. We subsequently requested CFHT Target-of-Opportunity observations of the source. The observations were carried out in the queued service observing mode on 2008 September 29, 30, October 3, and 4. The detector was the wide-field imager MegaCam, which consists of 36  $2048 \times 4612$  pixel<sup>2</sup> CCDs. The field of our target was imaged on CCD 22. The pixel scale is  $0.187''/\text{pixel}$ . A Sloan  $r'$  filter was used for imaging.

During the four nights, we obtained 60, 63, 84, and 72 images, respectively. The exposure time for each image was 20 s. The total observation times were 1.1, 1.2, 1.6, and 1.4 hours, respectively. The observing conditions in the first night were good, with an average seeing of  $0.8''$ . In the second night, the seeing condition was not good, having a large range of  $0.8$ – $1.8''$  and an average of  $1.1''$ . Therefore 6 images with large seeing values were excluded from the data. The third night had good observing conditions, with an average seeing of  $0.7''$ . The observing conditions in the fourth night were relatively variable, with the seeing in a range of  $0.6$ – $1.2''$  and an average of  $0.8''$ .

### 2.4. Data Reduction and Photometry

We used the IRAF packages for data reduction. The images were bias subtracted and flat fielded. We performed PSF-fitting photometry to measure the bright-

nesses of the source and other in-field stars. A photometry program DOPHOT (Schechter et al. 1993) was used.

Before photometry, we positionally calibrated our Gemini images (made during the quiescent state) to reduce possible contamination from the two nearby stars, since the two stars had similar brightnesses and were  $0.6''$  and  $1.0''$  away from the target (e.g., Wang et al. 2009). We first made a reference image by combining three best-quality  $i'$  images on August 7. All Gemini images were then calibrated to this reference image. We determined the positions of our target and the two nearby stars in the reference image and fixed them at these positions for photometry of the Gemini images. Differential photometry was performed to eliminate systematic flux variations in the images. Six isolated, non-variable bright stars in the field were used. The brightnesses of our targets and other stars in each frame were calculated relative to the total counts of the six stars. Standard stars 95-100 and 95-96 (Landolt 1992) were observed on August 4 and used for  $g'$  and  $i'$  flux calibration, respectively. To convert Landolt (1992) Vega magnitudes of the standard stars to Sloan filter magnitudes, transformation equations given by Fukugita et al. (1996) were used.

For CFHT data, because J1808.4 was in outburst, approximately 30 times brighter than in quiescence, and the exposure time was short, no effort was made to separate the two nearby stars from our target. Differential photometry was also performed, with 10 in-field bright stars used for calibrating out systematic flux variations among the images. No standard stars were requested in our CFHT program. Using 8 in-field bright stars, we flux calibrated our  $r'$  images to those in Wang et al. (2009).

## 2.5. Light Curve Results

The obtained Gemini and CFHT light curves are shown in Figure 1 and Figure 2, respectively. We note that during our Gemini observations, the source was brightening. Over two days, the source's  $g'$  and  $i'$  brightnesses changed by 1.3 and 0.9 mag, respectively. In addition, the amplitudes of modulation decreased from  $\simeq 0.4$  mag to  $\simeq 0.2$  mag.

At the time of the outburst, J1808.4 was visible to CFHT for only approximately one hour. Therefore each CFHT light curve covered half of the binary orbit. It can be seen that the first two light curves are sinusoidal-like with an amplitude of 0.2 mag, similar to those seen in quiescence. The latter two light curves changed to a smaller amplitude of 0.1 mag, and the average source brightness at the time decreased by approximately 0.3 mag.

## 3. FITTING

### 3.1. Light curve model

We fitted the data using the *Icarus*<sup>6</sup> light curve model for irradiated companions in binaries (Breton et al. 2012). The model was adapted from the code developed by van Kerkwijk (e.g. Stappers et al. 2001), and has been recently used for two other systems (van Kerkwijk et al. 2010a,b; Breton et al. 2012). The model is similar to the ELC program (Orosz & Hauschildt 2000) that was em-

ployed by Deloye et al. (2008) for their earlier work on J1808.4.

In this model, the surface of the companion is constructed by solving the hydrostatic equilibrium equation for a rotating body, which in our case was tidally locked to the neutron star. We implemented a new stellar grid parametrization that uses a triangle tessellation obtained from the subdivision of the primitives of an isocahedron. This parametrization yields uniform coverage on the projected sphere surrounding the star and allows for better performance of the code. We scaled the star so that its size matches that of the Roche lobe, which is justified from the fact that J1808.4 regularly undergoes outbursts involving mass transfer from the companion. A base temperature for the companion is chosen and effects of gravity darkening accounted using Lucy's law (Lucy 1967), with a power-law index of 0.08. To this, we apply the irradiative flux from the neutron star in the way prescribed by Orosz & Hauschildt (2000). Finally, we integrated over the visible surface the emerging flux in a selected photometric filter, which was interpolated from BTSettl atmosphere models (Allard et al. 2003, 2007, 2011), in order to obtain the total flux at a given orbital phase and for specific orbital parameters.

We approximated the disk contribution by adding an orbital-independent, constant value to the companion's flux. The disk flux values inferred at different photometric bands at one epoch constitute a spectral energy distribution, which were checked for consistency with arising from an accretion disk (§ 4.2). We also made the implicit presumption that the system is seen sufficiently face-on so that there is no mutual eclipse/shadow arising between the disk and the companion. This presumption is motivated by the fact that light curves of J1808.4 in quiescence are symmetrical and do not show obvious signs of flux changes that could result from the interaction between the two components (Wang et al. 2009). Moreover, the estimated orbital inclination from previous work (e.g., Deloye et al. 2008) as well as that inferred from this work (see § 3.5—the maximum value we found is only  $56^\circ$ ) indicates that the companion is unlikely to be obscured by the disk for any reasonable disk scale height.

### 3.2. Bayesian inference

We used a Bayesian framework to make statistical inferences on our light curve modeling parameters. The Bayesian inference on a set of parameters  $\vec{\theta}$  is obtained from their posterior probability, which is conditional to the prior knowledge,  $I$ , that we have of these parameters and the experimental data  $D$ . The posterior probability can be written as the product of the priors times the likelihood of the data:  $p(\vec{\theta}|I, D) = p(\vec{\theta}|I) p(D|\vec{\theta}, I)/p(D|I)$ , where the denominator is a normalization factor to ensure that the posterior probability integrated over the parameter space is unity [see Gregory (2005) for an introduction to Bayesian analysis].

### 3.3. Model parameters

#### INCLINATION AND RADIAL VELOCITY SEMI-AMPLITUDE

The X-ray timing of J1808.4 already provides accurate measurements of its orbital period and the projected

<sup>6</sup> Freely available at <https://github.com/bretonr/Icarus>.

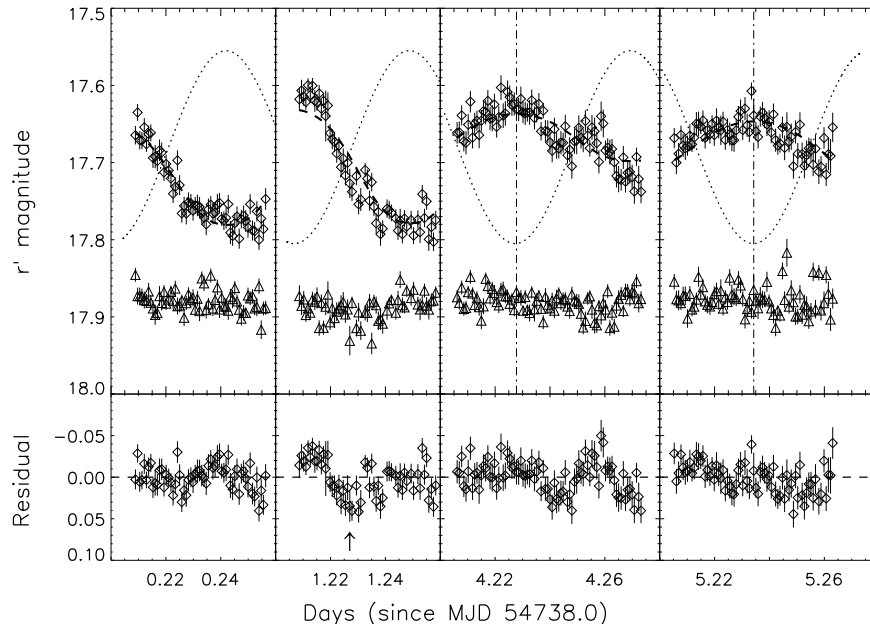


FIG. 2.— CFHT  $r'$  light curves of J1808.4 in the 2008 outburst (diamonds), with the last two up-shifted by 0.3 mag. For comparison, light curves of a comparison star are plotted as triangles. The X-ray ephemeris of the pulsar, which gives its mean orbital longitude (Hartman et al. 2008), is shown as dotted curves, and positions of superior conjunction of the companion are indicated in the last two panels (dash dot lines). Our model light curves are shown as dashed curves. In the residuals of the second light curve from our model fit, significant deviation of a few data points from our model is seen (marked by an arrow), indicating the modulation peak is narrower than that of our model.

semi-major axis of the neutron star. In order to fully parametrize the system (e.g. masses, separation, etc.), two additional quantities are required. We chose the orbital inclination,  $i$ , and the projected radial velocity semi-amplitude of the companion  $K_{\text{comp}}$ , because of their close connection to observables. For the orbital inclination, Deloye et al. (2008) found a relatively large range of  $36$ – $67^\circ$  ( $1\sigma$ ) from their fitting. Since a subset of the data used in our analysis included the data set from Deloye et al. (2008), we chose the priors to be flat in  $\cos i$  to fully search for the best-fit range in this work.

The use of spectroscopic observations to constrain the companion’s radial velocity is made quite difficult due to its faintness in quiescence. While the system does get much brighter during outbursts, its emission mainly contains features arising from the accretion disk. Using spectra obtained in the 2008 outburst and analyzing Doppler images of the N III  $\lambda 4640$  emission line associated to the Bowen blend, Cornelisse et al. (2009) and Elebert et al. (2009) both tracked the motion of the companion in J1808.4. Because the latter analyzed a total of 39 spectra, which included 16 spectra that were analyzed and reported by the former, we considered the result given by the latter,  $K_{\text{Bowen}} = 324 \pm 15 \text{ km s}^{-1}$ , and reported our fitting results based on this measurement. We discussed the influence of the different  $K_{\text{Bowen}}$  measurements to our fitting in § 5.1 by also considering the value obtained by Cornelisse et al. (2009),  $K_{\text{Bowen}} = 248 \pm 20 \text{ km s}^{-1}$ . However only unreasonably low-mass values for the neutron star were found from our fitting when the value of Cornelisse et al. (2009) was used.

The average location of the Bowen emission is indicated by  $K_{\text{Bowen}}$ , which is essentially produced on the ir-

radiated hemisphere of the star and has a different velocity from that of the center of mass,  $K_{\text{comp}}$ . Elebert et al. (2009) discussed the “K-correction” factor required to convert the Bowen velocity to the center of mass and estimated that  $K_{\text{comp}} = 370 \pm 40 \text{ km s}^{-1}$ , based on modeling by Muñoz-Darias et al. (2005).

We included the  $K_{\text{Bowen}}$  constraint as a Gaussian prior in our Bayesian inference. For every realization of the model, we determined the velocity of the companion’s light center by calculating the average velocity over the visible surface, weighted by the flux contribution of each surface element. Since the irradiated side of the companion is much hotter than that of the back side (6000 K vs. 3000 K, respectively), the flux contribution from the non-irradiated side in the  $g'$ -band becomes negligible and the inferred velocity should be a good approximation of  $K_{\text{Bowen}}$ . As expected from Muñoz-Darias et al. (2005), we found that  $K_{\text{comp}} \sim 370 \text{ km s}^{-1}$  is required to satisfy the velocity constraint. Such value is also consistent with the semi-analytical K-correction relationship derived by van Kerkwijk et al. (2010a) for the companion to PSR B1957+20, which shares similarities to J1808.4. From analytical and numerical modeling of this irradiated companion, they determined that the ratio of the observed projected light-center velocity to the projected center-of-mass velocity follows  $K_{\text{obs}}/K_2 = 1 - f_{\text{eff}} R_{\text{nose}}/a_2$ , where  $R_{\text{nose}}/a_2$  is the radius of the nose of the companion in units of separation to the system’s barycenter, and  $f_{\text{eff}} \sim 0.6$ , a parameter relatively independent of the system and companion properties such of orbital inclination, filling factor, and surface temperature as long as the companion is strongly irradiated and nearly fills its Roche lobe. Hence, for J1808.4

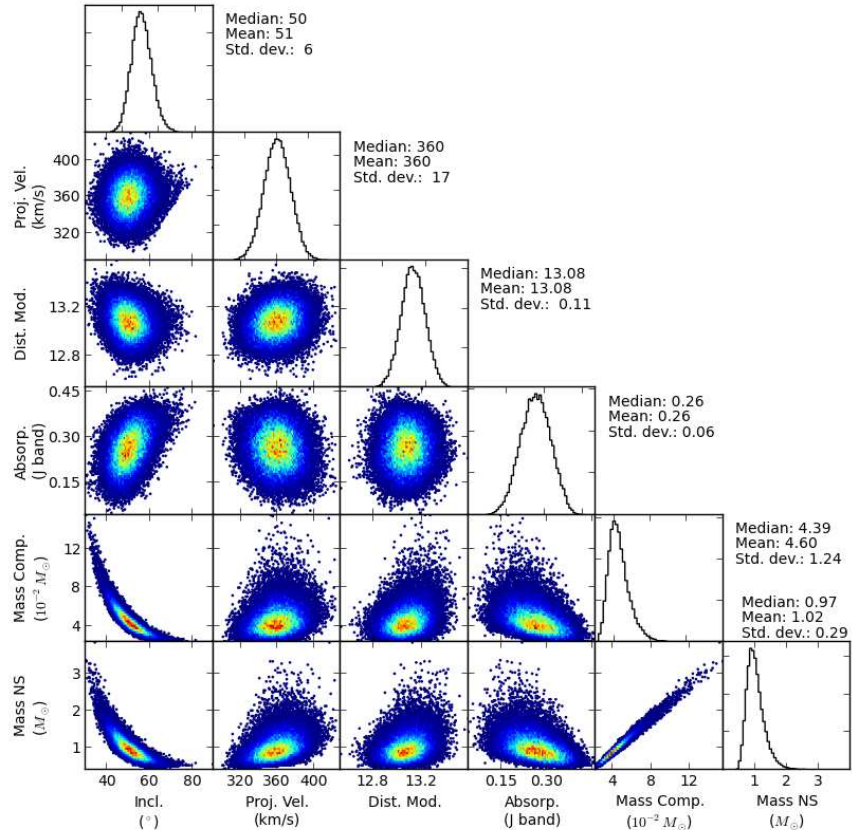


FIG. 3.— One- and two-dimensional distributions of the key parameter values resulting from our MCMC fitting. Values of the median, mean, and standard deviation of each parameter are given. The masses are inferred values from the neutron star mass function, the orbital inclination, and the projected velocity.

$R_{\text{nose}}/a_2 \sim 0.2$  which, again, implies a measurable velocity comparable to the above value.

#### BASE AND DAY-SIDE TEMPERATURES

The base temperature of the companion was fixed using a temperature-mass relationship for low-mass brown dwarfs (Deloye et al. 2008). The temperature, as a function of mass alone, ranges between 2000–3000 K. From the photometric colors near the inferior conjunction of the companion, we confirmed that the temperature is consistent with the range. In addition, keeping it a free parameter did not improve the light curve fits significantly.

We used flat priors for the companion’s day-side temperature since its surface albedo is uncertain as well as the amount of incident energy approximated by the pulsar’s spin-down energy. Although it is unlikely, we tested modeling the whole dataset with a constant day-side temperature. We found such a setting did not result in good fits. A separate day-side temperature for each observation was used in order to account for variability.

#### DISTANCE MODULUS AND REDDENING

Using several different methods, Galloway & Cumming (2006) estimated the distance  $d$  to J1808.4. First by setting the time-averaged X-ray flux equal to the expected mass transfer rate from gravitational radiation, they found a low limit of  $d > 3.4$  kpc. They also modelled the type I X-ray bursts that all

showed photospheric radius expansion during the 2002 October outburst of J1808.4, and obtained a distance range of  $d = 3.1 - 3.8$  kpc. Finally considering the peak flux of the radius expansion bursts as a standard candle,  $d = 3.6$  kpc was estimated for a pure helium atmosphere or  $d = 4.3$  kpc from an empirical value of Kuulkers et al. (2003). We set a Gaussian prior on the distance modulus  $DM = 12.72 \pm 0.15$ , where a 7% uncertainty was chosen in order to compensate for possible uncertainties in the distance estimates (see Galloway & Cumming 2006 for details).

For the reddening, we also chose a Gaussian prior and set the  $J$  band absorption to  $A_J = 0.21 \pm 0.05$  using the value derived from Wang et al. (2009).

#### DISK FLUX

The same as for the day-side temperature, we used an independent disk flux value with a flat prior for each set of continuous observation, as well as each photometric band. We designed our light curve fitting algorithm to optimize the disk flux value every time the companion parameters were changed. Since the disk contribution is an additive, linear problem in the flux system — and therefore a very simple non-linear problem in the magnitude system — solving for the best disk flux comes to the cost of only a few additional CPU cycles compared to the lengthier optimization of the companion parameters.

In the 2008 August 7 observation (Figure 1), a notice-

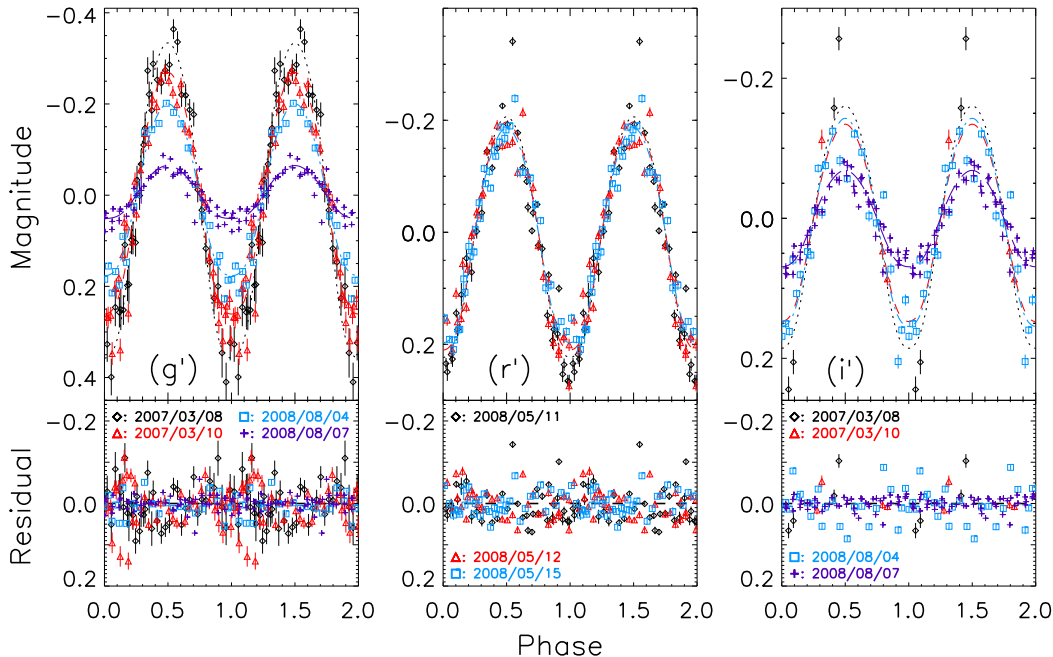


FIG. 4.— Folded quiescent light curves (at  $P = 7249.157$  s), with  $g'$ ,  $r'$ , and  $i'$  data shown in the left, middle, and right panel, respectively. Following the data sequence given in Table 1, the data are plotted as diamonds, triangles, squares, and plus signs, respectively, while the best-fit model light curves are plotted as dotted, dashed, dash-dot, and long dash curves, respectively. Two cycles are displayed for clarity.

able rise in the overall flux level is visible and likely indicates that J1808.4 was coming out of quiescence. Clearly, a constant flux value cannot account for this change and we allowed for a small linear variation of the disk contribution over the course of the observation.

#### NOISE PARAMETER

In order to account for intrinsic short-term flux variations that sometimes could significantly deviate away from the sinusoidal-like orbital modulation of J1808.4 (Deloye et al. 2008; Wang et al. 2009; see also § 4.1), we added a ‘noise parameter’ to the uncertainties of our data. The uncertainty of a flux datum  $i$  in dataset  $j$  becomes  $s_{ij} = \sqrt{b_j} \sigma_{ij}$ , where  $s_{ij}$  and  $\sigma_{ij}$  are the new and old uncertainties, respectively, and  $b_j$  is the noise parameter. This technique is commonly used in Bayesian analysis (see, e.g., Gregory et al. 1999; Gregory 2011) and has an effect loosely similar to that of uncertainties rescaling which is performed in frequentist analysis to obtain a reduced  $\chi^2 \sim 1$ . The priors are chosen to be logarithmic (i.e. Jeffrey’s priors) in order to provide equal weighting per decade since the noise term is a scaling parameter.

#### 3.4. MCMC fitting

The light curve fitting is a multi-dimensional nonlinear optimization problem that we tackled using an MCMC method (Gilks et al. 1995). This is particularly efficient to make Bayesian inference since the full posterior distribution is evaluated. In the limit that the observed magnitude errors are normally distributed, the likelihood function can be written as  $p(D|\vec{\theta}I) \propto \exp(-\chi^2/2)$ , where  $\chi^2$  is the conventional chi-square.

For the MCMC, we chose the *stretch move* algorithm that is part of a family of MCMC methods called

*ensemble samplers with affine invariance* described by Goodman & Weare (2009). In a nutshell, the algorithm is executed by simultaneously running several chains, all initialized at random locations of the parameter phase space. Every step of the MCMC, a move is proposed for each chain by choosing a complementary chain at random and drawing point along a line passing through the last position recorded in the two chains. How big a step away from the previous position is determined using a distribution which is affine invariant [i.e.,  $g(z^{-1}) = zg(z)$ ]. The proposed move is accepted with a probability that is slightly different than that of the usual Metropolis algorithm in order to satisfy the detailed balance requirement [see Goodman & Weare (2009) for the details]. An advantage of the stretch move algorithm is that the acceptance rate, which controls the efficiency of the chain, can be tuned using a single parameter in the proposal distribution, as opposed to one per dimension for a random walk Metropolis algorithm. It should also perform better for highly skewed and badly scaled distributions.

We ran the stretch move algorithm using 30 simultaneous chains for a total of 100 000 steps each. The proposal distribution’s tuning parameter was determined from a previous trial run and the obtained acceptance rates of the chains were found to be in the range 20 – 30%, as prescribed by Roberts & Rosenthal (2001). For subsequent analysis, we discarded the first 30 000 points (e.g., the burn-in period) and thinned the remaining by keeping every other 50 points in order to reduce the autocorrelation. In order to ensure that our MCMC has converged we visually inspected the trace of the parameters and performed the Geweke test (Geweke 1992) by comparing the mean of 10%-subsections of the first half of the chain to the remaining second half.



### 3.5. Results

We originally aimed to compare the modulations in quiescence and outburst by fitting the light curves separately. However the combination of the short light curves during the outburst and their relatively large uncertainties does not provide tight constraints. We also tested fitting all data together, but for the same reason the results were hardly changed compared to those including the quiescent data only. We therefore fit all the quiescent data obtained from 2007 March to 2008 August with our model. In Table 1, we provide a summary of the fit results as well as several additional quantities inferred from the marginalized posterior probabilities of our irradiated companion modeling. The one and two-dimensional posteriors are displayed in Figure 3.

We show all folded light curve data points, model light curves of the median parameter values, and residuals in Figure 4. As can be seen, our model generally reproduces the observations quite well with the data points evenly distributed along the model light curves. However it can be noted that a few light curves have relatively large variations around our model fits, which are also reflected by the noise parameter values. These variations, noted in previous studies (Deloye et al. 2008; Wang et al. 2009), were likely intrinsic and stochastic and can not be described by our current model.

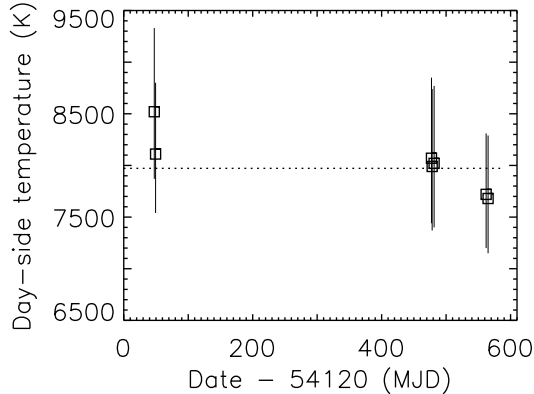


FIG. 5.— Day-side temperature of the companion star in J1808.4 as a function of time, which can be described by a constant of 7970 K (dotted line).

Our inferred orbital inclination,  $i = 50^{+6}_{-5}$  deg, is consistent with previous estimates from Deloye et al. (2008) and Cackett et al. (2009) (the latter found  $i = 55^{+8}_{-4}$  deg by relativistic Fe line fitting; see also Papitto et al. 2009; Patruno et al. 2009) despite the day-to-day disk and irradiated-side temperature variability, which probably impair our ability to combine multi-epoch data obtained in different bands. Consequently we constrained the neutron star and companion to have masses of  $0.97^{+0.31}_{-0.22} M_{\odot}$  and  $0.04^{+0.02}_{-0.01} M_{\odot}$ , respectively. Our fitting has narrowed the possible mass ranges for both the neutron star and companion and points to a low-mass neutron star in J1808.4, while we note with caution that the  $3\sigma$  range for the mass of the neutron star is still wide,  $0.47$ – $2.52 M_{\odot}$  (Table 1). In addition, we note that our measurement of  $M_{\text{ns}}$  is in agreement with the independent estimate of  $M_{\text{ns}} < 1.5 M_{\odot}$  from X-ray pulse shape

modeling (Morsink & Leahy 2011).

The results of the distance modulus and extinction,  $DM = 13.08 \pm 0.11$  and  $A_J = 0.26 \pm 0.06$ , are slightly larger than the previous estimates. The posteriors are very close to being normally distributed, and have standard deviations nearly the same as that of the priors. Our inferred companion’s projected radial velocity semi-amplitude,  $360^{+17}_{-16} \text{ km s}^{-1}$ , is in agreement with the value,  $370 \pm 40 \text{ km s}^{-1}$ , from Elebert et al. (2009). We observed that the uncertainty on  $K_{\text{comp}}$  is only 50% as large as that of the priors, which implies that the data contribute to constraining the companion’s velocity. The most likely reason is that given the distance and absorption are relatively well-determined, and the fact that the companion fills its Roche lobe, the observed luminosity constrains the actual radius of the companion which is tied up to its orbital velocity.

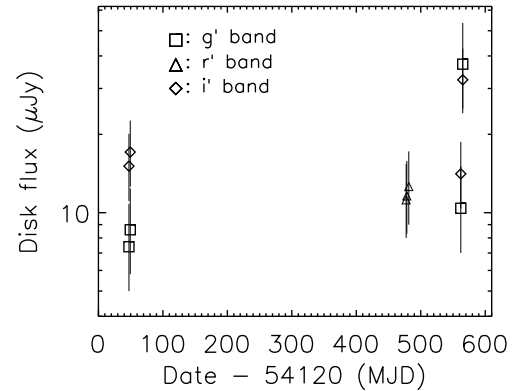


FIG. 6.— Disk flux contribution as a function of time. The squares, triangles, and diamonds indicate the  $g'$ ,  $r'$  and  $i'$ -band data, respectively.

The day-side temperatures of the companion are consistent with being a constant before the 2008 outburst (Figure 5), and we found that a temperature of  $7972 \pm 243 \text{ K}$  best fits them ( $\chi^2 = 1.1$  for 6 degrees of freedom). We note that the data points may suggest a trend of temperature decreasing over the time, but no conclusion can be drawn due to the large standard deviations. Our result is relatively surprising as one might have naively expected increased activity as the system was going towards an outburst. The behavior of the disk flux contribution (Figure 6) is also consistent with being constant in each band over time, except for the last observation (on 2008 Aug 7) in which the flux increased by a factor  $\gtrsim 2$  within 3 days. Detailed analysis of the disk components is given below in § 4.2.

Previously by fitting the first two sets of data (obtained on 2007 March 8 and 10; Table 1), Deloye et al. (2008) found  $M_{\text{ns}} > 1.8 M_{\odot}$ , which favoured a high-mass neutron star in J1808.4. Our results are drastically different, now pointing to a light,  $M_{\text{ns}} < 1.3 M_{\odot}$  neutron star. In addition to the constraint on the companion’s radial velocity from the  $K_{\text{Bowen}}$  measurements (see also the discussion in § 5.1), the causes of the difference can be understood from the following. Nearly simultaneous multi-band light curves are crucial in order to break parameter degeneracies and, for instance, tell

the stellar temperature apart from the orbital inclination (Breton et al. 2012), while Deloye et al. (2008) had very limited multi-band information of the binary (see § 2.1). The other important aspect is that the disk contribution acts as a DC component on an observed light curve and is almost completely degenerate with the orbital inclination. However, we were able to disentangle the orbital inclination from the disk in our data since the contribution from the latter varies over time whereas the orbital inclination remains constant. Finally our MCMC fitting allowed to efficiently explore the entire parameter space whereas Deloye et al. (2008) restricted their fitting to well-defined regions with a coarse grid.

### 3.5.1. Outburst results

Because of the reasons given above, we studied the outburst light curves by fitting them with all parameters of the binary system fixed at the median parameter values obtained from our fitting to the quiescent data (Table 1). The free parameters were only the day-side temperature of the companion and disk flux. In addition, to have sufficient constraints, the last two sets of the data were assumed to have one day-side temperature value (the average magnitudes of the source in the two days do not have a significant change). Our model generally fits the observed light curves, as can be seen in Figure 2, which shows the model light curves as well as residuals of the observed data points from them. From fitting, we found that the day-side temperature was in a range of 12,000–25,000 K and disk flux approximately 20–30 times larger than those in quiescence. These results are also given in Table 1. A test to use the fitting results from the quiescent data as priors was conducted, and consistent results were obtained.

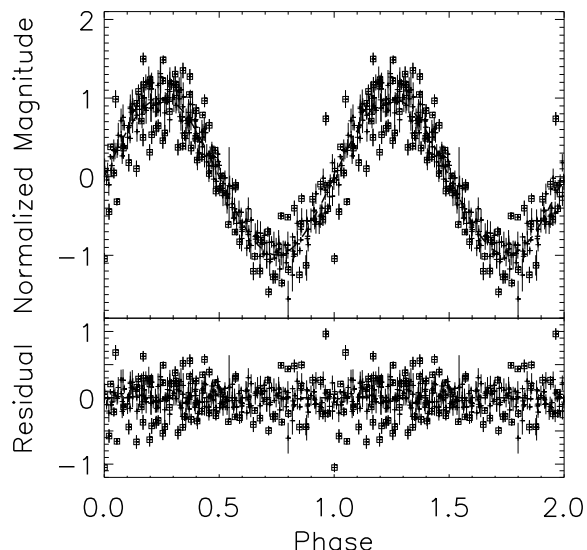


FIG. 7.— Normalized and folded multi-band light curves of J1808.4. The source’s multi-band light curves can generally be described by a sinusoid function, but contain a significant fraction of outliers. The data points marked by squares are those deviate from the best-fit sinusoid more than  $3\sigma$  away.

We note that while the overall shape of the modulations in the outburst is in general consistent with our model of an irradiated companion star, there are fine

structures in the outburst light curves. As can be seen in Figure 2, the second light curve is sinusoidal-like, but it appears to deviate systematically in the middle part from our model. In addition, the data points in the third and fourth ones are not accurately represented and the third one shows a second minor peak after the main peak. We conclude that minor modulation variations were detected in the outburst.

## 4. ANALYSIS

### 4.1. Orbital Period Determination

It has been shown that the orbital periodicity of J1808.4 can be determined from time-resolved photometry with a phase-coherent timing technique (Wang et al. 2009). Using three observations made in 5 days, Wang et al. (2009) have found an uncertainty of 2.8 s on the orbital period  $P$ . With this uncertainty, it can be inferred that such timing observations within a maximum time span of 3.6 month are needed in order to avoid losing track of the optical periodicity phase. Because our Gemini observations in 2008 August satisfies this requirement, which further improves the accuracy of the period measurement, we attempted to phase connect all our light curves obtained during the quiescent state. The orbital period of J1808.4 has been found to increase at a rate of  $1.2 \times 10^{-4} \text{ s yr}^{-1}$  from pulsar timing (Hartman et al. 2008; Di Salvo et al. 2008; Burderi et al. 2009; Hartman et al. 2009; Patruno et al. 2012), and this large value, which is not well understood because it is an order of magnitude larger than that predicted by standard theoretical calculations for such a binary (however see Patruno et al. 2012), might be confirmed from optical observations.

Since the modulation was variable over different bands and times of the observations (Figure 4), we fit each set/band of the light curves individually with a sinusoidal function  $m = m_c + m_h \sin[2\pi(t/P + \phi_0)]$  (where  $t$  is time,  $\phi_0$  the starting phase, and  $P$  is the orbital period fixed at 7249.157 s), subtracted the obtained constant magnitude  $m_c$  from them, and normalized them with the obtained semi-amplitudes  $m_h$ . The uncertainties resulting from this normalization were added in quadrature to the original uncertainties of the magnitudes. The normalized light curves were then fit with a single sinusoid again, and we found that the best-fit has an orbital period  $P = 7249.151 \pm 0.003 \text{ s}$ , while  $\chi^2 = 3170$  for 331 degrees of freedom. The large  $\chi^2$  value reflects systematic uncertainties resulting from photometry, intrinsic scattering of the data points from a single sinusoid (Wang et al. 2009), and probably errors from normalizing short light curves. In Figure 7, the folded light curve, best-fit sinusoid, and residuals to the sinusoid are shown. A few data points deviating more than  $3\sigma$  from the sinusoid are marked by squares. We estimated the uncertainties by scaling them by  $(\chi^2/\text{DoF})^{1/2}$  and obtained  $P = 7249.150 \pm 0.008 \text{ s}$  and  $\phi_0 = 0.675 \pm 0.003$  at MJD 54599.0 (TDB), where phase  $\phi = 0.0$  corresponds to the ascending node of the pulsar orbit. These results are consistent with that obtained from pulsar timing (Hartman et al. 2009) within the uncertainties. Since the measurement accuracy of a period is generally proportional to the length of the time span, it is unlikely to be able to measure the orbit change rate via long-term optical photometry of the source.



#### 4.2. Accretion Disk During Our Observations

The accretion disk components resulting from our MCMC fitting are shown as a function of wavelengths in Figure 8. The data points before the onset of the brightening on 2008 Aug. 7 can be reproduced by a simple accretion disk model, whose structure in quiescence is known to be different from that of the standard, steady-state disk model (e.g., Dubus, Hameury, & Lasota 2001; Baptista & Bortoletto 2004). In both states the temperature profile can be described by an exponential function,  $T(r) \propto r^\xi$ , where  $r$  is disk radius, but the former is usually flatter than the latter ( $\xi = -0.75$  is the standard value for the latter case). We fit the quiescent data points with the temperature profile. Free parameters were disk temperature at  $r = 10^{10}$  cm,  $T_{10}$ , and  $\xi$ . Source distance, reddening, and inclination angle were fixed at the median values found from our MCMC fitting, and the inner and outer edges of the disk were assumed to be at the light cylinder of the pulsar ( $\simeq 1.2 \times 10^7$  cm) and 90% of the Roche-lobe radius of the pulsar ( $\simeq 3.2 \times 10^{10}$  cm; Frank et al. 2002), respectively. We found that  $T_{10} = 6200^{+100}_{-200}$  K and  $\xi = -0.5 \pm 0.1$  provide the best-fit (the minimum  $\chi^2 = 0.3$  for 7 degrees of freedom). The small  $\chi^2$  value reflects the large standard deviations of the data points. The spectrum of the best-fit disk model is shown as the solid curve in Figure 8.

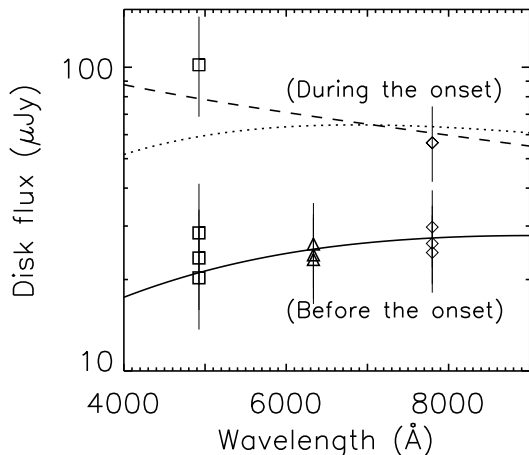


FIG. 8.— Broad-band spectra of the disk component in J1808.4. Squares, triangles, and diamonds indicate the  $g'$ ,  $r'$ , and  $i'$  data, respectively. The spectral data points before the onset of the brightening (from 2007 Mar 8 to 2008 Aug 4) can be described by an accretion disk that has temperature profile  $T(r) \propto r^\xi$  with  $\xi = -0.5$  (solid curve). During the onset (on 2008 Aug 7), a  $\xi = -0.5$  model (dotted curve) can still describe the onset data points, while a steeper,  $\xi \sim -0.8$ , temperature profile (dashed curve) can also be considered.

The data points on Aug. 7 are 2–4 times brighter than those obtained three days earlier, indicating the onset of the disk brightening. In addition, there is possibly a spectral change from rising to falling although we have only two data points and their standard deviations are too large for such a conclusion to be drawn. For example if  $\xi = -0.5$  is fixed (the same as that obtained above in quiescence), the disk model with  $T_{10} = 8200 \pm 700$  K provides a best fit (the minimum  $\chi^2 = 1.4$  for 1 de-

gree of freedom), which is plotted as the dotted curve in Figure 8. For a comparison, a steeper profile such as  $\xi = -0.8$  ( $T_{10} = 8300$  K) is also plotted (the dashed curve) in the figure. We note that the brightness at the time (average  $i' \simeq 19.9$ ) was approximately 7 times lower than that at the outburst peak (average  $i' \simeq 17.8$ ; Elebert et al. 2009). It is of great interest to study how the disk evolved during the one and a half month period from Aug 7 to September 22 directly preceding the reported X-ray outburst detection. Since J1808.4 is known to have an outburst every 3 yrs (Galloway 2008), a close monitoring of the source before an outburst might help us learn the disk evolution over such a period.

### 5. DISCUSSION

#### 5.1. Influence of the Companion Radial Velocity

Since the orbital period  $P$  and the projected semi-major axis of the J1808.4 pulsar have been accurately measured from X-ray timing (Chakrabarty & Morgan 1998; Hartman et al. 2009), the semi-amplitude of the pulsar's projected velocity  $K_1$  is known. Combining with it, the  $K_{\text{comp}}$  measurement from optical spectroscopy provides a strong constraint on properties of the binary, particularly the neutron star's mass  $M_{\text{ns}}$ . It can be shown that

$$M_{\text{ns}} = \frac{1}{2\pi G} \frac{K_{\text{comp}}^3 P}{(1 + K_1/K_{\text{comp}})^2} \frac{1}{\sin^3 i} \quad ,$$

where  $G$  is the gravitational constant. If  $K_{\text{comp}}$  is known,  $M_{\text{ns}}$  is determined only by the orbital inclination  $i$  (similar discussions were also given by Cornelisse et al. 2009 and Elebert et al. 2009). This  $M_{\text{ns}}-i$  relation is shown in Figure 9, with 68% and 99.7% confidence-level regions resulting from our fitting (low left panel in Figure 3) overplotted. As can be seen, our fitting results are consistent with the analytical expectations.

If  $K_{\text{comp}} = 299 \pm 23$  km s $^{-1}$  instead, as reported by Cornelisse et al. (2009), the  $M_{\text{ns}}-i$  relation is expected to shift toward lower values. We explored this effect by fitting our model using  $K_{\text{Bowen}} = 248 \pm 20$  km s $^{-1}$  (Cornelisse et al. 2009) as a prior. As expected, we found similar results but noticeably  $i = 45 \pm 5^\circ$  and  $M_{\text{ns}} = 0.58^{+0.20}_{-0.14} M_\odot$  (both uncertainties are  $1\sigma$ ), which are both smaller than the values obtained using the Elebert et al. (2009) measurement as the prior. The neutron star now has an unrealistically low mass. In Figure 9, we show the obtained  $M_{\text{ns}}-i$  regions from our fitting in detail. As a result of the change of  $K_{\text{Bowen}}$  to the smaller value, the regions are shifted accordingly, but only the upper corner of the  $3\sigma$  region allows  $\geq 1 M_\odot$  neutron star mass. This suggests that their measurement is in general too low to provide a realistic mass range for the neutron star.

On the basis of the current  $K_{\text{comp}}$  measurements,  $K_{\text{comp}} \leq 410$  km s $^{-1}$ , since the K-correction factor is derived assuming that  $K_{\text{Bowen}}$  indicated the orbital motion of the  $L1$  point. Therefore from our fitting,  $M_{\text{ns}} \leq 1.3 M_\odot$  at  $1\sigma$  level, which confirms the point raised analytically by Cornelisse et al. (2009) and Elebert et al. (2009) that a light neutron star in J1808.4 is favored.

#### 5.2. Modulation in the Outburst

While our short coverage of the outburst modulation prevents us from conclusive analysis, we have likely detected modulation changes during the outburst. The second light curve appears to systematically deviate from the simple sinusoidal-like shape, as seen in Figure 2. This deviation could have been caused by disk flux variations during the outburst, with a timescale of 20 min. On the other hand, a modulation with a narrower flux peak can also explain this. For example using our model, we qualitatively tested this and found that narrower light curves can indeed be produced with smaller irradiated areas, although much higher temperatures are required to account for similar maximum luminosity. It is plausible that during the outburst, a hot spot could have formed on the surface of the companion due to strong irradiation by X-rays from the central pulsar.

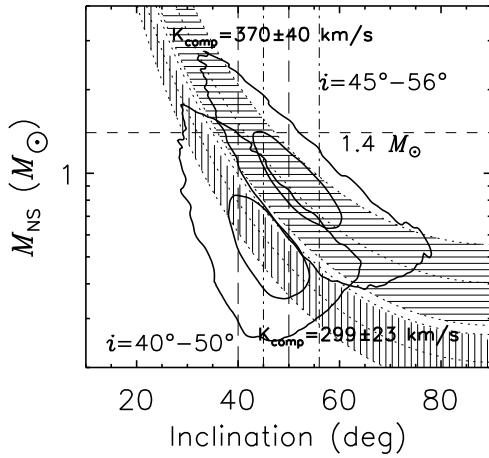


FIG. 9.—  $M_{\text{NS}}$  vs.  $i$  for  $K_{\text{comp}} = 370 \pm 40 \text{ km s}^{-1}$  (Elebert et al. 2009) and  $K_{\text{comp}} = 299 \pm 23 \text{ km s}^{-1}$  (Cornelisse et al. 2009). For the first and latter values, the 1- and 3- $\sigma$  constraints on  $M_{\text{NS}}$  and  $i$ , resulting from our fitting, are overplotted as upper-right and lower-left contours, respectively. The derived 1- $\sigma$   $i$  value ranges are also indicated by vertical dash-dot and long dashed lines for the first and latter  $K_{\text{comp}}$  values, respectively.

The third and fourth light curves, 3 days after the second one, changed to have a modulation with 0.1 mag amplitude. Elebert et al. (2009) have reported their detection of a slow-rise and a fast-decline modulation on 2008 Oct. 1, which would strongly suggest the appearance of superhump modulation since or at least on Oct. 1 (Retter et al. 1997; Wang & Chakrabarty 2010). As observed in cataclysmic variables (CVs), superhumps do often appear a few days after the start of an outburst (or superoutburst as in CVs). Before an accretion disk dumps nearly all its stored mass to the companion, the disk in the beginning of the outburst expands beyond the 3:1 resonance radius, which induces the tidal instability. As a result, the disk develops into an eccentric form, producing superhump modulation (e.g., see Osaki 1996 for details). However in our data, not only are the light curves significantly different from that obtained on Oct. 1 by Elebert et al. (2009; for example, its modulation amplitude was 0.2 mag), but also no clear phase shift of the modulation is seen. In the last two panels of Figure 2, we marked superior conjunction of the companion (i.e., when the pulsar is at  $270^\circ$  from the ascending

node) with two vertical dash-dotted lines, and as can be seen, the maximums of the modulation were in phase with superior conjunction of the companion. For superhump modulation in J1808.4 and given its mass ratio  $q = 0.04/1.0$ , the expected phase shift would be 0.1 per day, estimated from the empirical relation between superhump and orbital periods and  $q$  among known superhump binaries (Patterson et al. 2005; Wang et al. 2009).

Our last two outburst light curves are similar to that obtained on Oct. 7/8 by Elebert et al. (2009). We note that there is marginal evidence that an additional component appears in the third light curve and that a weak trend exists in the residuals of the fourth light curve from our model fit. Although the 0.1 mag amplitude modulation was in phase with that of the companion, we speculate that it could consist of modulation components such as from the disk but that modulation from the companion still dominated at the time. In order to understand this modulation, better observational coverage of the source’s outbursts and detailed analysis of each component’s possible modulation should be needed. In any case, given that the modulation showed significant variations over a few days, further observational studies of the source’s modulation over its future outbursts are warranted.

### 5.3. Albedo of the Companion Star

The day-side optical emission from the companion is due to reprocessing of energy flux from the central pulsar. The required irradiation luminosities in quiescence in our model were in a range of  $(8\text{--}12) \times 10^{33} \text{ erg s}^{-1}$ . The known energy output from the pulsar in quiescence consists of its rotational energy loss rate  $L_{\text{sd}}$  and X-ray emission, where the latter is two orders of magnitude lower than the former. Therefore the energy output absorbed by the companion is approximately  $(1 - \eta_*)f_b L_{\text{sd}} \simeq 9 \times 10^{33}(1 - \eta_*)f_b \text{ erg s}^{-1}$ , where  $\eta_*$  is the albedo of the companion in quiescence and  $f_b$  is defined as the beaming factor for the pulsar’s emission towards the companion. Comparing this value to the irradiation luminosity range,  $\eta_* \simeq 0$  is required if  $f_b \simeq 1$  (isotropic emission case). However from similar studies of black widow pulsar binaries (Stappers et al. 2001; Reynolds et al. 2007),  $\eta_*$  was found to be around 0.6. If this value is taken for our case,  $f_b \approx 2.5$  beaming for the pulsar’s energy emission would be required.

Recently Takata et al. (2012) have proposed a model that irradiation could be due to  $\gamma$ -ray emission from pulsars for APMP systems in quiescence. According to their calculations for J1808.4, a high-mass ( $\sim 2 M_\odot$ ) neutron star is preferred considering that the irradiation luminosity is  $L_\gamma \sim 10^{34} \text{ erg s}^{-1}$ . Their model is therefore not fully supported by our derived limits on the neutron star’s mass but compatible within  $3\sigma$ .

The required irradiation luminosity during the outburst on 2008 Sept. 29 was found to be  $6.2 \times 10^{35} \text{ erg s}^{-1}$ , while the data on the other three nights are not considered because of the deviation of their modulations from a simple sinusoid-like shape. Nearly at the same time (MJD 54738.28), the 2.5–25 keV X-ray luminosity of the pulsar was  $3.2 \times 10^{36} \text{ erg s}^{-1}$  (Hartman et al. 2009), where 4.1 kpc source distance (Table 1) is used. Comparing the two values, the X-ray albedo of the companion  $\eta_X \simeq 0.8$  for the  $f_b \simeq 1$  isotropic emission case. Such a

large albedo value has been found in studies of accretion disks' X-ray reprocessing (de Jong et al. 1996). On the other hand, if  $\eta_X \simeq 0.6$  still holds,  $f_b \simeq 1/2$  would be required. The difference in the albedo or beaming factor during quiescence and the outburst probably provides additional evidence for having a different heating source in the quiescent state.

## 6. SUMMARY

We have obtained nearly simultaneous  $g'$  and  $i'$  light curves of J1808.4 in 2008 August and  $r'$  light curves in 2008 September/October, respectively before and after the reported 2008 September 22 X-ray outburst. In the former datasets, we detected a clear disk brightening as the optical precursor of the X-ray outburst. In the latter datasets, the sinusoidal orbital flux modulation was observed to have an amplitude decrease from 0.2 mag to 0.1 mag.

We employed an MCMC technique to fit all the quiescent data, which include those previously published in Deloye et al. (2008) and Wang et al. (2009), with an irradiated companion model. We found a tight constraint on the inclination angle of the binary system:  $i = 50^{+6}_{-5}$  deg. The resulting constraints on the masses of the neutron star and companion were found to be  $0.75\text{--}1.28 M_\odot$  and  $0.03\text{--}0.06 M_\odot$ , respectively. These results rely on the  $K_{\text{comp}}$  measurement, which currently is not certain, but (conservatively) considering  $K_{\text{comp}} \leq 410 \text{ km s}^{-1}$ , we found  $M_{\text{ns}} \leq 1.3 M_\odot$  in J1808.4.

From our fitting, the derived day-side temperature of the companion appeared to be constant over the period of  $\sim 500$  days during which our quiescent data were obtained. The derived disk components can be described by a simple disk temperature profile, while a change to a steeper spectrum was possibly seen at the onset of the disk brightening.

No modulation changes that might clearly reveal a different heating source during the outburst were found from our observations. Minor modulation variations, including a change of amplitude from 0.2 mag to 0.1 mag,

were detected in our outburst data. We have possibly found a narrower modulation peak than that seen in quiescence in one set of our data, which could be caused by the existence of a hot spot on the surface of the companion due to intense irradiation by the X-ray pulsar. In order to further study these variations, good observational coverage of the source during its outbursts is needed.

The Gemini queue mode observations were carried out under the program GS-2008B-Q-9. The Gemini Observatory is operated by the Association of Universities for Research in Astronomy, Inc., under a cooperative agreement with the NSF on behalf of the Gemini partnership: the National Science Foundation (United States), the Science and Technology Facilities Council (United Kingdom), the National Research Council (Canada), CONICYT (Chile), the Australian Research Council (Australia), CNPq (Brazil), and CONICET (Argentina). The CFHT observations were carried out under the TOO program 08BD97, obtained with MegaPrime/MegaCam, a joint project of CFHT and CEA/DAPNIA, at the Canada-France-Hawaii Telescope (CFHT) which is operated by the National Research Council (NRC) of Canada, the Institut National des Sciences de l'Univers of the Centre National de la Recherche Scientifique of France, and the University of Hawaii.

We thank Jacob M. Hartman for providing us the X-ray flux data during the 2008 outburst of J1808.4 and anonymous referee for valuable suggestions, and RPB thanks Rutger van Haasteren for discussions about MCMC. This research was supported by the starting funds of Shanghai Astronomical Observatory, National Basic Research Program of China (973 Project 2009CB824800), and National Natural Science Foundation of China (11073042). ZW is a Research Fellow of the One-Hundred-Talents project of Chinese Academy of Sciences. COH is supported by an Ingenuity New Faculty Award and an NSERC grant.

*Facility:* Gemini:South (GMOS), CFHT (MegaPrime/MegaCam)

## REFERENCES

- Allard, F., Allard, N. F., Homeier, D., Kielkopf, J., McCaughrean, M. J., & Spiegelman, F. 2007, *A&A*, 474, L21
- Allard, F., Guillot, T., Ludwig, H.-G., Hauschildt, P. H., Schweitzer, A., Alexander, D. R., & Ferguson, J. W. 2003, *IAU Symp.* 211, Brown Dwarfs, ed. E. Martin (Cambridge: Cambridge Univ. Press), 325
- Allard, F., Homeier, D., & Freytag, B. 2011, *Astronomical Society of the Pacific Conference Series*, 448, 91
- Baptista, R., & Bortoletto, A. 2004, *AJ*, 128, 411
- Breton, R. P., Rappaport, S. A., van Kerkwijk, M. H., & Carter, J. A. 2012, *ApJ*, 748, 115
- Burderi, L., Di Salvo, T., D'Antona, F., Robba, N. R., & Testa, V. 2003, *A&A*, 404, L43
- Burderi, L., Riggio, A., Di Salvo, T., Papitto, A., Menna, M. T., D'Ai A., & Iaria, R. 2009, *A&A*, 496, L17
- Cackett, E. M., Altamirano, D., Patruno, A., Miller, J. M., Reynolds, M., Linares, M., & Wijnands, R. 2009, *ApJ*, 694, L21
- Campana, S. et al. 2004, *ApJ*, 614, L49
- Campana, S., et al. 2002, *ApJ*, 575, L15
- Chakrabarty, D., & Morgan, E. H. 1998, *Nature*, 394, 346
- Cornelisse, R., et al. 2009, *A&A*, 495, L1
- D'Avanzo, P., Campana, S., Casares, J., Covino, S., Israel, G. L., & Stella, L. 2009, *A&A*, 508, 297
- D'Avanzo, P., Campana, S., Covino, S., Israel, G. L., Stella, L., & Andreuzzi, G. 2007, *A&A*, 472, 881
- de Jong, J. A., van Paradijs, J., & Augusteijn, T. 1996, *A&A*, 314, 484
- Deloye, C. J., Heinke, C. O., Taam, R. E., & Jonker, P. G. 2008, *MNRAS*, 391, 1619
- Di Salvo, T., Burderi, L., Riggio, A., Papitto, A., & Menna, M. T. 2008, *MNRAS*, 389, 1851
- Dubus, G., Hameury, J.-M., & Lasota, J.-P. 2001, *A&A*, 373, 251
- Elebert, P., et al. 2009, *MNRAS*, 395, 884
- Frank, J., King, A., & Raine, D. J. 2002, *Accretion Power In Astrophysics* (Cambridge University Press)
- Fukugita, M., Ichikawa, T., Gunn, J. E., Doi, M., Shimasaku, K., & Schneider, D. P. 1996, *AJ*, 111, 1748
- Galloway, D. 2008, in *American Institute of Physics Conference Series*, Vol. 983, 40 Years of Pulsars: Millisecond Pulsars, Magnetars and More, 510–518
- Galloway, D. K., & Cumming, A. 2006, *ApJ*, 652, 559
- Geweke, J. 1992, in *IN BAYESIAN STATISTICS* (University Press), 169–193
- Gilks, W. R., Richardson, S., & Spiegelhalter, D. J. 1995, *Markov Chain Monte Carlo in Practice*, 1st edn. (Chapman and Hall/CRC)

- Goodman, J., & Weare, J. 2009, *Communications in Applied Mathematics & Computational Science*, 5, 65
- Gregory, P. C. 2005, *Bayesian Logical Data Analysis for the Physical Sciences: A Comparative Approach with 'Mathematica' Support* (Cambridge University Press)
- Gregory, P. C. 2011, *MNRAS*, 415, 2523
- Gregory, P. C., Peracaula, M., & Taylor, A. R. 2009, *ApJ*, 520, 376
- Hartman, J. M., Patruno, A., Chakrabarty, D., Markwardt, C. B., Morgan, E. H., van der Klis, M., & Wijnands, R. 2009, *ApJ*, 702, 1673
- Hartman, J. M., et al. 2008, *ApJ*, 675, 1468
- Hauschildt, P. H., Allard, F., & Baron, E. 1999, *ApJ*, 512, 377
- Heinke, C. O., Jonker, P. G., Wijnands, R., Deloye, C. J., & Taam, R. E. 2009, *ApJ*, 691, 1035
- Heinke, C. O., Jonker, P. G., Wijnands, R., & Taam, R. E. 2007, *ApJ*, 660, 1424
- Homer, L., Charles, P. A., Chakrabarty, D., & van Zyl, L. 2001, *MNRAS*, 325, 1471
- Hook, I. M., Jørgensen, I., Allington-Smith, J. R., Davies, R. L., Metcalfe, N., Murowinski, R. G., & Crampton, D. 2004, *PASP*, 116, 425
- Jonker, P. G., Torres, M. A. P., & Steeghs D. 2008, *ApJ*, 680, 615
- Kuulkers, E., den Hartog, P. R., in't Zand, J. J. M., Verbunt, F. W. M., Harris, W. E., Cocchi, M. 2003, *A&A*, 399, 663
- Landolt, A. U. 1992, *AJ*, 104, 340
- Lucy, L. B. 1967, *ZAp*, 65, 89
- Markwardt, C. B., & Swank, J. H. 2008, *The Astronomer's Telegram*, 1728, 1
- Morsink, S. M. & Leahy, D. A. 2011, *ApJ*, 726, 56
- Muñoz-Darias, T., Casares, J., & Martínez-Pais, I. G. 2005, *ApJ*, 635, 502
- Orosz, J. A., & Hauschildt, P. H. 2000, *A&A*, 364, 265
- Osaki, Y. 1996, *PASP*, 108, 39
- Papitto, A., Di Salvo, T., D'A, A., Iaria, R., Burderi, L., Riggio, A., Menna, M. T., & Robba, N. R. 2009, *A&A*, 493, L39
- Patruno, A., Rea, N., Altamirano, D., Linares, M., Wijnands, R., & van der Klis, M. 2009, *MNRAS*, 396, L51
- Patruno, A. 2010, *ArXiv e-prints*
- Patruno, A., Bult, P., Gopakumar, A., Hartman, J. M., Wijnands, R., van der Klis, M., & Chakrabarty, D. 2012, *ApJ*, 746, L27
- Patterson, J., et al. 2005, *PASP*, 117, 1204
- Reynolds, M. T., Callanan, P. J., Fruchter, A. S., Torres, M. A. P., Beer, M. E., & Gibbons, R. A. 2007, *MNRAS*, 379, 1117
- Retter, A., Leibowitz, E. M., & Ofek, E. O. 1997, *MNRAS*, 286, 745
- Roberts, G. O., & Rosenthal, J. S. 2001, *Statist. Sci.*, 16, 351
- Schechter, P. L., Mateo, M., & Saha, A. 1993, *PASP*, 105, 1342
- Stappers, B. W., van Kerkwijk, M. H., Bell, J. F., & Kulkarni, S. R. 2001, *ApJ*, 548, L183
- Takata, J., Cheng, K. S., & Taam, R. E. 2012, *ApJ*, 745, 100
- van Kerkwijk, M. H., Breton, R., & Kulkarni, S. R. 2010a, *ArXiv e-prints*
- van Kerkwijk, M. H., Rappaport, S. A., Breton, R. P., Justham, S., Podsiadlowski, P., & Han, Z. 2010b, *ApJ*, 715, 51
- Wang, Z., Bassa, C., Cumming, A., & Kaspi, V. M. 2009, *ApJ*, 694, 1115
- Wang, Z., & Chakrabarty, D. 2010, *ApJ*, 712, 653
- Wang, Z., et al. 2001, *ApJ*, 563, L61
- Wijnands, R., & van der Klis, M. 1998, *Nature*, 394, 344

TABLE 1  
FITTED AND DERIVED MODEL PARAMETERS

| Parameter                                 | Median | 68.3% interval | 99.7% interval | Reduced $\chi^2$ <sup>a</sup> | DoF |
|---|--------|----------------|----------------|-------------------------------|-----|
| Inclination (degree)                      | 50     | 45–56          | 34–72          | ...                           | ... |
| $K_{\text{comp}}$ (km s <sup>-1</sup> )   | 360    | 344–377        | 311–410        | ...                           | ... |
| Distance modulus                          | 13.08  | 12.97–13.19    | 12.74–13.41    | ...                           | ... |
| Absorption (J-band)                       | 0.26   | 0.20–0.32      | 0.09–0.42      | ...                           | ... |
| 2007 Mar 8 (MJD 54167.35; Gemini/GMOS-S)  |        |                |                |                               |     |
| Day-side Temp. (K)                        | 8520   | 7870–9330      | 6960–11310     | ...                           | ... |
| Disk $g'$ ( $\mu\text{Jy}$ )              | 7.4    | 5.0–10.8       | 0.9–27.1       | ...                           | ... |
| Noise                                     | 2.3    | 1.8–2.9        | 1.2–5.0        | 1.0                           | 40  |
| Disk $i'$ ( $\mu\text{Jy}$ )              | 15.1   | 11.1–20.1      | 2.3–38.9       | ...                           | ... |
| Noise <sup>b</sup>                        | 19.0   | 9.6–46.8       | 1.7–441.3      | 0.74                          | 4   |
| 2007 Mar 10 (MJD 54169.35; Gemini/GMOS-S) |        |                |                |                               |     |
| Day-side Temp. (K)                        | 8110   | 7540–8800      | 6680–10540     | ...                           | ... |
| Disk $g'$ ( $\mu\text{Jy}$ )              | 8.6    | 5.8–12.4       | 1.0–30.3       | ...                           | ... |
| Noise                                     | 6.7    | 5.4–8.4        | 3.6–14.0       | 1.0                           | 44  |
| Disk $i'$ ( $\mu\text{Jy}$ )              | 17.1   | 12.6–22.6      | 2.7–43.4       | ...                           | ... |
| Noise                                     | 5.3    | 2.7–11.9       | 0.7–75.0       | 0.83                          | 4   |
| 2008 May 11 (MJD 54597.32; Gemini/GMOS-S) |        |                |                |                               |     |
| Day-side Temp. (K)                        | 8070   | 7440–8850      | 6530–10780     | ...                           | ... |
| Disk $r'$ ( $\mu\text{Jy}$ )              | 11.2   | 8.0–15.4       | 1.7–32.5       | ...                           | ... |
| Noise                                     | 32.5   | 25.6–41.5      | 16.6–74.1      | 0.97                          | 36  |
| 2008 May 12 (MJD 54598.34; Gemini/GMOS-S) |        |                |                |                               |     |
| Day-side Temp. (K)                        | 7990   | 7370–8740      | 6460–10540     | ...                           | ... |
| Disk $r'$ ( $\mu\text{Jy}$ )              | 11.6   | 8.3–15.8       | 1.7–33.1       | ...                           | ... |
| Noise                                     | 13.6   | 10.7–17.5      | 7.0–31.8       | 0.98                          | 36  |
| 2008 May 15 (MJD 54601.38; Gemini/GMOS-S) |        |                |                |                               |     |
| Day-side Temp. (K)                        | 8020   | 7400–8770      | 6510–10610     | ...                           | ... |
| Disk $r'$ ( $\mu\text{Jy}$ )              | 12.6   | 9.0–17.2       | 1.8–36.2       | ...                           | ... |
| Noise                                     | 12.7   | 10.0–16.3      | 6.4–29.9       | 1.0                           | 36  |
| 2008 Aug 4 (MJD 54682.08; Gemini/GMOS-S)  |        |                |                |                               |     |
| Day-side Temp. (K)                        | 7720   | 7200–8310      | 6400–9650      | ...                           | ... |
| Disk $g'$ ( $\mu\text{Jy}$ )              | 10.4   | 7.0–15.1       | 1.3–36.3       | ...                           | ... |
| Noise                                     | 26.3   | 19.6–36.0      | 11.5–76.5      | 0.93                          | 23  |
| Disk $i'$ ( $\mu\text{Jy}$ )              | 14.1   | 10.4–18.7      | 2.2–36.0       | ...                           | ... |
| Noise                                     | 35.8   | 26.6–49.1      | 15.4–102.9     | 1.0                           | 24  |
| 2008 Aug 7 (MJD 54685.12; Gemini/GMOS-S)  |        |                |                |                               |     |
| Day-side Temp. (K)                        | 7680   | 7150–8290      | 6350–9770      | ...                           | ... |
| Disk $g'$ ( $\mu\text{Jy}$ )              | 37.2   | 25.1–53.6      | 4.8–127.3      | ...                           | ... |
| Noise                                     | 21.4   | 17.4–26.6      | 12.0–43.1      | 0.96                          | 47  |
| Disk $i'$ ( $\mu\text{Jy}$ )              | 32.4   | 24.1–42.7      | 5.6–81.3       | ...                           | ... |
| Noise                                     | 7.6    | 6.2–9.4        | 4.2–15.0       | 1.0                           | 48  |
| Outburst data                             |        |                |                |                               |     |
| 2008 Sept 29 (MJD 54738.21; CFHT/MegaCam) |        |                |                |                               |     |
| Day-side Temp. (K)                        | 22870  | 22200–23510    | 20740–24720    | ...                           | ... |
| Disk $r'$ ( $\mu\text{Jy}$ )              | 292.3  | 291.6–293.0    | 290.2–295.3    | ...                           | ... |
| Noise                                     | 1.6    | 1.3–1.9        | 0.9–2.9        | 0.94                          | 60  |
| 2008 Sept 30 (MJD 54739.21; CFHT/MegaCam) |        |                |                |                               |     |
| Day-side Temp. (K)                        | 24830  | 24560–24950    | 23630–25000    | ...                           | ... |
| Disk $r'$ ( $\mu\text{Jy}$ )              | 292.6  | 292.4–293.0    | 292.3–294.8    | ...                           | ... |
| Noise                                     | 3.2    | 2.6–3.9        | 1.9–5.9        | 1.0                           | 57  |
| 2008 Oct 3 (MJD 54742.21; CFHT/MegaCam)   |        |                |                |                               |     |
| Day-side Temp. (K)                        | 12530  | 11960–13090    | 10820–14180    | ...                           | ... |
| Disk $r'$ ( $\mu\text{Jy}$ )              | 240.4  | 239.6–241.2    | 237.0–243.9    | ...                           | ... |
| Noise                                     | 1.7    | 1.5–2.0        | 1.1–2.8        | 1.0                           | 84  |
| 2008 Oct 4 (MJD 54743.21; CFHT/MegaCam)   |        |                |                |                               |     |
| Disk $r'$ ( $\mu\text{Jy}$ )              | 238.1  | 237.2–239.1    | 234.0–242.3    | ...                           | ... |
| Noise                                     | 1.6    | 1.4–1.9        | 1.0–2.8        | 1.0                           | 72  |
| Inferred Parameters                       |        |                |                |                               |     |
| Mass Comp. ( $M_{\odot}$ )                | 0.04   | 0.03–0.06      | 0.02–0.11      | ...                           | ... |
| Mass NS ( $M_{\odot}$ )                   | 0.97   | 0.75–1.28      | 0.47–2.52      | ...                           | ... |

<sup>a</sup> The quoted reduced- $\chi^2$  were calculated at the median parameter values, and are provided for indicative purposes only since they do not take into account the priors nor full Bayesian posterior distributions.

<sup>b</sup> Noise parameter  $b$  (see 3.3)